PCCP

ROYAL SOCIETY OF CHEMISTRY

Competition between Salt Bridge and Non-Zwitterionic Structures in Deprotonated Amino Acid Dimers

SCHOLARONE™
Manuscripts

Competition between Salt Bridge and Non-Zwitterionic Structures in Deprotonated Amino Acid Dimers

Sven Heiles[a,b]*, Giel Berden[c], Jos Oomens[c,d] and Evan R. Williams[a]*

a Department of Chemistry, University of California, Berkeley, California 94720-1460, United States

b Institute of Inorganic and Analytical Chemistry, Justus-Liebig-University Giessen, 35392 Giessen, Germany

c Radboud University Nijmegen, Institute for Molecules and Materials, FELIX Laboratory, Toernooiveld 7c, 6525 ED Nijmegen, The Netherlands

d Van't Hoff Institute for Molecular Sciences, University of Amsterdam, Science Park 904, 1098 XH Amsterdam, The Netherlands

*Address correspondence to Dr. Sven Heiles and Prof. Evan R. Williams:

Institute of Inorganic and Analytical Chemistry
Justus Liebig University Giessen, Giessen, Germany
email: sven.heiles@anorg.chemie.uni-giessen.de

Department of Chemistry
University of California, Berkeley, USA
e-mail: erw@berkeley.edu

Abstract

Structures of deprotonated Cys, Asp, Glu, Phe, Pro, His homo dimers as well as [2Cys-3H]⁻, [Asp+Glu-H]⁻ and [2Glu-2H+Na]⁻ are investigated with infrared multiple-photon dissociation (IRMPD) spectroscopy between 650 and 1850 cm⁻¹ and theory. The IRMPD spectra of all investigated complexes but [2His-H]⁻, [2Phe-H]⁻ and [2Pro-H]⁻ indicate that the structures consist of a neutral non-zwitterionic (NZ) and a deprotonated form of the amino acids. In contrast, the spectrum of [2His-H]⁻ is complex and indicates the presence of multiple isomers and/or interactions between His and [His-H]⁻, so that its structure differs from that of the other deprotonated amino acid dimers. For [2Phe-H]⁻ and especially for [2Pro-H]⁻, some IRMPD bands can only be explained by the presence of salt bridge (SB) structures in the dimer in which a deprotonated amino acid interacts with a zwitterionic neutral amino acid. Computational results indicate that SB structures are lower in energy at 298 K than corresponding NZ structures for neutral-anion complexes in which SB formation is not disrupted by amino acid side chains or conformational constraints, such as in [2Glu-H]⁻ and [2Cys-3H]⁻ for which NZ structures are most consistent with experimental results. For deprotonated amino acid dimers in which these interfering interactions are absent, such as in [2Phe-H]⁻ and [2Pro-H]⁻, the higher number of hydrogen bonds in SB compared to NZ structures stabilize the formation of zwitterionic neutral amino acids and consequently SB structures in agreement with results from IRMPD spectroscopy. These results suggest that SB structures likely occur in deprotonated peptide or protein ions at hydrophobic sites, such as protein-protein interfaces or in the interior of proteins, where interfering functional groups will not disrupt SB formation.

Introduction

The interactions of amino acid (AA) residues with each other and their environments play a central role in the chemistry and structures of peptides and proteins. Neutral AAs, for example, are zwitterions in aqueous solution, whereas these AAs are non-zwitterionic (NZ) in isolation.[1–3] Interactions of isolated AAs with metal cations,[4–13] halide anions,[14,15] an electron,[16] water molecules[17–19] or protonated amines,[20–22] can stabilize the zwitterionic (ZW) forms of some AAs over corresponding NZ structures. In solution, basic and acidic AA residues of peptides and proteins with ionized side chains can be stabilized by inter- and intramolecular interactions. These ionized AA residues play an important role in the structures, solubilities and reactivities of peptides and proteins owing to long-range Coulombic interactions of these groups with distant residues or solvent molecules. Charged groups in close proximity can form salt bridges (SBs) in which protonated and deprotonated AA residues interact directly. The formation of SBs in proteins in solution is well-known and SBs can stabilize or destabilize the native forms of proteins[23–25] and the interactions between proteins at protein-protein interfaces.[26,27] For gaseous peptides and protein ions, extensive evidence indicates that intramolecular SBs can exist in a solvent deficient environment.[28–38] Recent results from Julian and co-workers showed that photoelectron transfer dissociation (PETD) can be used to identify zwitterion pairs or SBs in peptides and protein ions.[32]

Because SBs influence reactivities and structures of peptides and proteins in solution and in the gas phase, the factors that are important contributors to SB stabilization, such as gas phase basicity,[4–6,11,39,40] gas phase acidity[9] and charge-solvation,[10,41] have been investigated in great detail. These investigations were mainly performed with AAs, small peptides and their complexes for which the number of inter- and intramolecular interactions are limited and

3

detailed theoretical investigations are feasible. Proton bound hetero- and homo-dimers of AAs,[42–48] protonated AA-amine[20,22,49] and AA-metal ion complexes[4–8,50] were used to investigate the propensity of AAs to form ZW or SB structures. For example, Arg, the AA with the highest gas phase basicity, and its dimers have been studied extensively to understand SB stabilization in the gas phase.[4,5,19,48,51,52] The proton bound Arg dimer forms a SB structure which is facilitated by extensive hydrogen bonding and electrostatic interactions between carboxylate and guanidinium groups.[48] Hydrogen bonding and Coulombic interactions also stabilize SBs in protonated Arg containing dipeptides but the propensity for proton transfer from acidic groups to the Arg side chain strongly depends on relative AA gas phase basicity.[53] The structure of $[HisArg+H]^+$ has a protonated C-terminal carboxylic acid group, whereas $[ArgArg+H]^+$ preferentially forms a SB structure. For $[GlyArg+M]^+$ and $[ArgGly+M]^+$ (M=H, Li, Na, K, Cs), SB formation occurs when charged groups involved in SB formation are effectively shielded by neighboring functional groups indicating that not only gas phase basicity but also conformational preferences of dipeptides, that are altered due to alkali metal attachment and peptide sequence, influence SB stability.[54] Findings for SB model systems are transferable to larger gas phase ions of biochemical relevance as evident from results for bradykinin, a nonapeptide with N- and C-terminal Arg residues.[32–38] Compelling evidence from blackbody infrared radiative dissociation (BIRD),[33] H/D exchange,[34] ion mobility measurements,[35,36] theory[37,38] and most recently PETD experiments[32] show that singly and doubly protonated bradykinin ions form SB structures in which charged residues are solvated by hydrogen bonding and electrostatic interactions from nearby functional groups. For other AAs, the propensity to form SB structures in positive ions is lower than that of Arg,[6,8,9,20–22,43–47,49,50,55–62] but metal ion or protonated amine complexation can stabilize ZW over NZ AA structures.[8,49] These results, however, depend on ion size[8] and relative

gas phase basicity[49] of the binding partners. The energetic difference between the NZ and ZW

forms of AA complexes in the gas phase are $0 - 20$ kJ/mol[19,21,49] and in some rare cases up to

~60 kJ/mol.[8] This indicates that there is a fine balance between ZW and NZ AA isomers and that

subtle variations of interaction patterns or the number of binding partners can drive AAs from

NZ to ZW structures and *vice versa*.

A large body of work for protonated/cationized AAs or peptides as model systems for

zwitterion/SB formation exists, but model systems with a net negative charge have only scarcely

been studied, despite the fact that most proteins carry an overall negative charge under

physiological conditions.[63] Zwitterion formation of anionic Gly radicals was shown to occur in

the presence of at least five water molecules by photoelectron spectroscopy,[18] consistent with

theoretical results that predict stabilization of the ZW relative to the NZ form by electron

attachment to neutral AAs.[16] In addition, Arg-halide anion complexes form ZW structures in the

gas phase[15,64] in contrast to results for negative tripeptide-halide complexes for which only

charge solvated structures are found in experiment.[65] The interaction between a neutral and a

deprotonated AA in the gas phase and their propensity to form SB structures has so far only been

studied for [2Gly-H]$^-$ and [2Gly-2H+Na]$^-$.[66] Spectroscopic results for [2Gly-H]$^-$ clearly show that

the neutral ZW Gly interacts with [Gly-H]$^-$ to predominantly form SB structures. In striking

contrast, the NZ isomer is 11 kJ/mol more stable than the SB structure in the protonated form of

this dimer, [2Gly+H]$^+$.[44] The energetic cost for zwitterion formation in [2Gly-H]$^-$ is compensated

by electrostatic interactions between opposite charges and hydrogen bonding that stabilize the

SB over the NZ form in this solvent deficient environment.[66]

In this work, [2Xxx-H]$^-$ (Xxx = Cys, Pro, Phe, His, Glu, Asp), [2Cys-3H]$^-$, [Asp+Glu-H]$^-$ and

[2Glu-2H+Na]$^-$ are investigated with IRMPD spectroscopy and theory, in order to develop a

better understanding for the factors that influence SB formation in anionic AA dimers. Despite

the limited spectral resolution of IRMPD spectroscopy compared to IR-UV double resonance[67]

or cryogenic ion spectroscopy,[68] IRMPD spectroscopy has provided detailed information on SB

formation in numerous positive AA and peptide ion model systems[4,5,7,19,22,42,44–47,50,53–56,58–61,66]

and, thus, appears to be well-suited for performing the first systematic investigation of negative

AA dimers. IRMPD spectra of negative AA dimers are compared to previously reported IR

spectra of compounds with well-known structures allowing assignments of all experimental

bands except for [2His-H]⁻ and [2Phe-H]⁻, [2Pro-H]⁻. For the latter two AA dimers, formation of

SB structures are discussed in the context of SB stabilizing hydrogen bond and electrostatic

interactions and for all other investigated AA dimers the influence of AA side chains on SB

stability is evaluated.

Computational and experimental methods

Computational

   Conformational searches using Macromodel 9.1 (Schrödinger Inc., Portland, OR, U.S.A.)

employing the OPLS2005 force field were performed in order to identify low-energy structures.

The candidate structures were grouped into families based on hydrogen bonding motif and amino

acid conformation. The lowest-energy structure of each structural family was subsequently

geometry optimized using quantum chemical methods resulting in four to eight lowest-energy

candidate structures. All quantum chemical calculations were performed in QChem.[69] The 6-

311++G** basis set was used for all atoms except sulfur for which the CRENBL basis set and

relativistic pseudopotential was employed (6-311++G**/CRENBL basis set combination

abbreviated by GCR). All electronic energies and geometries were computed at the B3LYP/GCR,

ωB97-D/GCR [70] or MP2/GCR level of theory. Vibrational frequencies were computed at the

B3LYP/GCR and ωB97-D/GCR level of theory. Electronic energies, unscaled harmonic

vibrations and rotational constants were used to calculate the relative thermodynamic stability,

i.e., the Gibbs free energy difference between isomers ΔG, as a function of temperature (0-350

K). An example for ΔG as a function of temperature for [2Pro-H]⁻ isomers is shown in **Figure S1**.

To compute ΔG for MP2/GCR results, the corresponding harmonic B3LYP/GCR frequencies

were used. Only the values at 0 and 298 K are reported in this manuscript. Binding energies for

lowest-energy SB and NZ negative amino acid dimer structures were computed at the MP2/GCR

level of theory, using the counterpoise correction method to account for the basis set

superposition error and to avoid overestimating the binding energies.[71] These energy values are

reported at 0 K and include zero-point vibrational energies contributions from B3LYP/GCR

computations. Harmonic vibrational spectra were convolved with Gaussian functions of 40 cm⁻¹

full width at half maximum and scaled with a uniform scaling factor of 0.987 (B3LYP/GCR) and

0.975 (ωB97-D /GCR) in order to compare calculated to experimental results.

Experimental

   All experiments were performed using a 4.7 T Fourier-transform ion cyclotron resonance (FT-

ICR) mass spectrometer equipped with a Micromass Z-spray electrospray ionization (ESI)

source and coupled to the free electron laser for infrared experiments (FELIX). Ions of

phenylalanine, cysteine, glutamic acid, aspartic acid and proline (Sigma-Aldrich) were produced

by ESI from 2 – 5 mM methanol/water (~80/20) solutions containing 1% aqueous ammonium

hydroxide solution (NH$_4$OH) or 1% NaOH to form negative deprotonated or doubly

deprotonated-sodiated amino acid dimers. A spray voltage of -2.5 kV and a flow rate of the

syringe pump of (5-10) μL/min were used. Ions were accumulated for ~4 s in a hexapole ion trap

before guiding and trapping the ions in the FT-ICR. Subsequently, the target complex was isolated by stored waveform inverse Fourier transform isolation. The isolated ions were irradiated by IR light from the FELIX light source for 2 s which led to their dissociation whenever the IR frequency was in resonance with a vibration of the trapped ions. The laser, operating at a macropulse rate of 5 Hz and with an energy of 15 – 60 mJ/pulse was attenuated to avoid saturation of the dissociation signal for the strongest vibrational bands. Three to six mass spectra were summed for every frequency step and FELIX was scanned from 650 to 1850 cm^{-1} in steps of 5 cm^{-1}. By plotting the normalized IRMPD rate constant $k=-ln(A/A_0)/t$ where A, A_0 and t are the precursor abundance, the summed precursor and product abundance and the irradiation time, respectively, as a function of wavenumber and correcting for the laser power, IRMPD spectra were obtained.

Results and discussion

IRMPD of negative amino acid dimers. Upon the absorption of IR photons, negative amino acid (AA) dimers [2Xxx-H]$^-$, Xxx = Gly,[66] Cys, Asp, Glu, Pro, Phe and His dissociate exclusively by loss of a neutral AA. The mixed dimer [Glu+Asp-H]$^-$ dissociates upon IRMPD to produce the two fragment ions, [Glu-H]$^-$ and [Asp-H]$^-$ in equal abundances indicating that these amino acids have nearly identical gas-phase acidities. The neutral loss of AAs as the only fragmentation pathway for [2Xxx-H]$^-$ (Xxx = Gly,[66] Cys, Asp, Glu, Pro, Phe and His) and [Glu+Asp-H]$^-$ is consistent with relatively weak non-covalent interactions between the constituent monomers in these complexes. Weaker non-covalent interactions preferentially break in IRMPD experiments thereby reducing or preventing cleavage of covalent bonds.[22,42,47,61,72] This is supported by the IRMPD results for the negative AA dimer [2Glu-2H+Na]$^-$ and the molecule [2Cys-3H]$^-$. In the former, carboxylate-sodium interactions likely contribute to the

strong interactions and in the latter, there is a covalent disulfide bond between the amino acids. IRMPD experiments of [2Glu-2H+Na]⁻ and [2Cys-3H]⁻ yield product ions assigned to [Glu-H]⁻, [Glu-H$_2$O-H]⁻, [Glu-2H+Na]⁻ and [Cys-H]⁻, [Cys+S-H]⁻, respectively. This indicates that cleavages of covalent bonds occur upon IRMPD if negative AA dimers are not just held together by weaker non-covalent interactions.

   IRMPD spectra of deprotonated amino acid dimers. IRMPD spectra were obtained for [2Xxx-H]⁻, Xxx = Gly,[66] Cys, Asp, Glu, Pro, Phe and His, [2Cys-3H]⁻, as shown in **Figure 1**, and [Glu+Asp-H]⁻ and [2Glu-2H+Na]⁻, see **Figure S2**. The IRMPD spectra are remarkably similar to each other over the spectral range between 650 and 1850 cm⁻¹. The similarity for [2Cys-H]⁻ /[2Cys-3H]⁻, [2Glu-H]⁻/[2Asp-H]⁻ and [2Phe-H]⁻/[2Pro-H]⁻ is not surprising, because the AA pairs only differ by an additional disulfide bridge, one side-chain CH$_2$ group and the aliphatic side chain, respectively.

   Each spectrum has three intense features (dashed lines, **Figure 1**) but the band width and band position for each spectral feature depends on the AA identity. The maximum of the highest energy band is located between 1690 cm⁻¹ and 1760 cm⁻¹. For [2Glu-H]⁻, [2Pro-H]⁻ and [2His-H]⁻, the band maximum is at 1743 cm⁻¹, 1691 cm⁻¹ and 1761 cm⁻¹, respectively. This suggests that the frequency of this band is strongly influenced by bonding interactions and bonding arrangements between the neutral and the deprotonated AA. In contrast, the maximum of the second intense band at ~1600 cm⁻¹ depends to a lesser extent on the AA identity. For [2Phe-H]⁻, the band is centered at 1602 cm⁻¹, whereas the largest shift of this band occurs for [2Glu-H]⁻ for which the spectral feature has its maximum intensity at 1586 cm⁻¹. The full width at half maximum of this band, however, varies from 51 cm⁻¹ for [2Phe-H]⁻ to 85 cm⁻¹ for [2Cys-3H]⁻. Interestingly, the bandwidth of the high energy band (1690 – 1760 cm⁻¹) is only broadened for [2Pro-H]⁻ (58 cm⁻¹)

as compared to ~45 cm^{-1} for all other negative AA dimers. The local chemical environment of functional groups or fluxional hydrogen bonds can increase the linewidth of bands in IR spectra of gas phase ions.[73,74]

The third spectral feature that all IRMPD spectra of the deprotonated AA dimers have in common is broad, asymmetric and has a maximum intensity between 1380 cm^{-1} and 1330 cm^{-1}, but extends to ~1470 cm^{-1} for [2Asp-H]$^-$ and ~1050 cm^{-1} for [2Pro-H]$^-$ on the high and low energy side of the maximum intensity (**Figure 1**). Whereas the band system centered at ~1360 cm^{-1} most likely consists of several features that are not resolved in the IRMPD spectra, pairs of negative AA dimers with similar band position, width and appearance are identifiable. Spectral band intensity and width of the band at ~1360 cm^{-1} for [2Cys-H]$^-$/[2Cys-3H]$^-$, [2Glu-H]$^-$/[2Asp-H]$^-$ and [2Phe-H]$^-$/[2Pro-H] are similar suggesting that the chemical environment and/or bonding of the functional group that give rise to this band are similar for these pairs of AA dimers.

In addition to the three spectral bands found in all negative AA dimer IRMPD spectra, features at ~900 cm^{-1} for [2Cys-H]$^-$, [2Cys-3H]$^-$, [2Phe-H]$^-$ and [2His-H]$^-$, between 900 – 1200 cm^{-1} for [2His-H]$^-$ and at ~1480 cm^{-1} for [2Phe-H]$^-$ and [2His-H]$^-$ (black dot, **Figure 1**) are present. Because these bands are only manifest in a few spectra, they are most likely associated with specific AA side chains and corresponding functional groups.

Assignment of IRMPD spectral features. Assignment of bands in IRMPD spectra is possible by comparisons to previously reported IR spectroscopy results of related compounds that have similar functional groups. Band assignments based on comparison between experimental and predicted IR spectra are summarized in **Table S2-S6**. For negatively charged AA dimers in the spectral range between 650 cm^{-1} and 1850 cm^{-1}, band assignment is particularly important for

vibrational modes associated with carboxylic acid, carboxylate and $-NH_2/-NH_3^+$ groups. For some deprotonated AA dimers no data is available below 1000 cm^{-1} which, however, does not affect the discussion of the most intense vibrational features of the IRMPD spectra. Displacement vectors for diagnostic vibrational normal modes involving these groups along with previously reported band centers are shown in **Figure 2**.[7,8,46,72,75–80]

   Free carbonyl C=O stretches of carboxylic acids are centered around 1780 cm^{-1} but can, depending on the extent of hydrogen bonding to the carbonyl oxygen, red shift down to ~1715 cm^{-1}. Because the highest energy band in the IRMPD spectra of all negative AA dimers except [2Pro-H]$^-$ are between 1714 cm^{-1} and 1761 cm^{-1} (**Figure 1**), this spectral feature is attributed to the carboxylic acid carbonyl C=O stretch. This assignment is also consistent with results for proton bound AA dimers for which the C=O stretch is between 1710 and 1775 cm^{-1} depending on the involvement of the –COOH group's carbonyl in hydrogen bonding interactions.[42,46,47] For proton bound AA dimers, multiple C=O bands are often assigned to differing chemical environments of –COOH groups or the presence of multiple isomers.[42,46,47] Because there is a maximum of one –COOH group in all negative AA dimers but [2Glu-H]$^-$ and [2Asp-H]$^-$, the linewidth of ~45 cm^{-1} for the C=O stretching features suggests that all –COOH groups experience similar chemical environments, *i.e.,* there is only one major binding mode to the carboxylic acid's C=O group. Even for [2Glu-H]$^-$ and [2Asp-H]$^-$ that contain more than one –COOH group, the C=O stretch bandwidths are ~45 cm^{-1}. This is most likely due to a similar average hydrogen bond environment of all –COOH groups.

   Only for [2Pro-H]$^-$, the appearance and position of the high-frequency band deviates from previously reported carboxylic acid C=O stretch positions and from all other negative AA dimers studied here (**Figure 1**). The band maximum and width is 1691 cm^{-1} and 58 cm^{-1}, respectively.

The greater line width of the spectral feature of [2Pro-H]$^-$ at 1691cm^{-1} could indicate the presence of multiple isomers or fluxional hydrogen bonds. In a recent IRMPD study of the proton bound cysteine dimer by Ieritano *et al.,* a feature at 1701 cm^{-1} was assigned to a –COOH group complexed by –NH$_3^+$.[42] In addition, von Helden and co-workers attributed bands at ~1705 cm^{-1} to C=O stretches where –NH$_3^+$ strongly interacts with carboxylic acids.[46] This is also consistent with IRMPD bands of carboxylic acids at ~1700 cm^{-1} in cationized AAs due to strong C=O···metal ion interactions.[81] For [2Pro+H]$^+$ and [Pro+Na]$^+$, bands at 1692 cm^{-1} and 1698 cm^{-1} were assigned to –COO$^-$ groups involved in SB formation.[47,56,82] We recently showed that [2Gly-H]$^-$ predominantly forms SB structures and a spectral feature at 1704 cm^{-1} is observed.[66] This combined experimental evidence strongly suggests that the 1691 cm^{-1} band in the IRMPD spectrum of [2Pro-H]$^-$ is due to –NH$_3^+$···O=C interactions and consequently indicates the formation of a SB, also consistent with theoretical predictions at different levels of theory (**Figure 2**, **Figure S3-4**, **Table S1**).

Other bands can also be assigned based on previously reported IR spectra. The spectral feature at ~1600 cm^{-1} in all negative AA dimer IRMPD spectra is consistent with anti-symmetric carboxylate stretching modes. Depending on the –COO$^-$ group's involvement in bonding interactions, the band is located between 1650 – 1540 cm^{-1} (**Figure 2**) in IR spectra.[76–78] Because this band is at ~1600 cm^{-1} in all spectra (**Figure 1**), hydrogen bonding to –COO$^-$ most likely occurs. This assignment is also supported by the IRMPD spectrum of [2Glu-2H+Na]$^-$ (**Figure S2**). [2Glu-2H+Na]$^-$ most likely has one additional –COO$^-$ group compared to [2Glu-H]$^-$ and the band at ~1600 cm^{-1} is significantly higher in intensity in the former compared to the latter spectrum. The band position of the –NH$_3^+$ scissoring mode typically coincides with the –COO$^-$ band and could also contribute to the experimental band at 1600 cm^{-1}.[46] The umbrella mode of

the ammonium moiety ($-NH_3^+$) for proton bound AA dimers is at ~1500 cm^{-1}, but only [2Phe-H]$^-$ and [2His-H]$^-$ spectra show sharp features (black dot, **Figure 1**) in this spectral region.[42,46] For [2Phe-H]$^-$, the band at 1489 cm^{-1} is consistent with the previously reported spectrum of deprotonated Phe which was assigned to vibrational modes of the phenyl-ring.[75] However, the same feature is absent in some spectra of Phe containing dipeptides and cationized Phe.[81] For [2His-H]$^-$ the band at 1470 cm^{-1} is consistent with spectral features of cationized His and is probably due to imidazole vibrations.[62]

The system of bands at ~1360 cm^{-1} in the spectra of all negative amino acid dimers is most likely associated with multiple vibrational modes. Due to spectral congestion, disentangling contributions from individual vibrational modes is very challenging, but based on previously published results, C-O-H bending vibrations (1440 – 1380 cm^{-1}),[46,72] symmetric $-COO^-$ stretching vibrations (1420 – 1300 cm^{-1})[76–78,83] and C-O stretching vibrations (1270 – 1120 cm^{-1})[46,72] may all contribute to the broad feature. Additional spectral features attributed to AA side chain functional groups appear for some deprotonated AA dimers. For example, a feature at ~900 cm^{-1} is present in IRMPD spectra of [2Phe-H]$^-$, [2Cys-H]$^-$ and [2Cys-3H]$^-$. Only [2His-H]$^-$ shows a very rich spectral structure between 650 and 1400 cm^{-1}. Because the gas phase spectra of His containing dipeptides,[53,84] cationized His,[62] His-halide complexes[15] and condensed phase spectra of imidazole[85] cannot explain all features in the spectrum of [2His-H]$^-$ in this spectral range, and because the spectrum does not resemble those of other negative AA dimers, it is likely that multiple isomers coexist or binding between the AAs differs for His from that for all other complexes.

Structures of deprotonated amino acid dimers. The computed lowest energy binding motifs of the negative AA homo-dimers [2Xxx-H]$^-$ (Xxx = Cys, Glu, Pro, Phe and His) and [2Cys-3H]$^-$

are non-zwitterionic (NZ) or salt bridge (SB) structures for which deprotonation and ZW

formation occurs at the AA backbone functional groups. NZ dimer structures contain a neutral

(non-zwitterionic) AA that binds via its carboxyl proton to a deprotonated AA`s carboxylate

group. SB dimers form due to the interaction of a neutral ZW AA with a deprotonated AA

(**Figure 3+4**). Because ZW AAs contain $-NH_3^+$ and $-COO^-$ groups, the preferred interaction

between deprotonated and ZW AAs in SB isomers occurs between hydrogen atoms of the

positive ammonium group and the oxygen atom(s) of the carboxylate group of the deprotonated

AA. Corresponding lowest energy NZ and SB isomers for the some negative AA dimers at the

B3LYP/GCR level of theory are shown in **Figure 3+4**. The hydrogen bond length between the

interacting AAs for NZ and SB isomers is affected by the AA side chains. For the NZ isomers,

the $-O\cdots H\text{-}O-$ distance increases from 1.39 Å for [2Cys-H]⁻ to 1.48 Å for [2Cys-3H]⁻ and is

smaller for AAs with an aliphatic side chain, *e.g.,* 1.33 Å for [2Pro-H]⁻. A similar trend of the

hydrogen bond length increase between AA moieties by interfering interactions with side chain

functional groups is observed for the SB structures (**Figure 3+4**). For example, [2Phe-H]⁻ has a

1.59 Å hydrogen bond (HB) in contrast with the shortest HB of 1.65 Å in [2Glu-H]⁻. This

indicates that in addition to the interactions between $-NH_3^+$ and $-COO^-$ groups in SB isomers

and $-COOH$ and $-COO^-$ groups in NZ isomers, further hydrogen bonding interactions, side chain

dispersion interactions, *i.e.,* "steric effects", or conformational constraints ([2Cys-3H]⁻) influence

the shortest hydrogen bond lengths between the AAs and the associated overall binding energies.

Factors influencing NZ vs. SB stability. One factor that can stabilize SB over NZ isomers are

hydrogen bonding interactions.[66] A qualitative way to characterize the contribution of hydrogen

bonding to the interaction strength between two AAs is by the overall number of inter- and

intramolecular HBs. Based on the functional groups participating in hydrogen bonding and

corresponding binding energies, HBs can be grouped into three categories. Namely, HBs

between two neutral groups (neutral HBs, NHBs, bond energy ~20 kJ/mol), ionic hydrogen

bonds (IHBs)[86–88] with bond energies between 20 – 150 kJ/mol and zwitterionic hydrogen bonds

(ZHBs). For the latter HB type, computational results predict a bond energy of ~105 kJ/mol.[66]

Therefore, the bond strength ranking is NHB < IHB ≤ ZHB. The corresponding number of HBs

with bond lengths less than 2.30 Å are shown in **Figure 3+4** for each isomer. All SB dimer

structures have more ZHBs and/or have an overall greater number of NHBs compared to the

corresponding NZ dimer structures. For example, the NZ and SB form of [2Phe-H]⁻ comprise a

total of 3 and 3 hydrogen bonds out of which 0 and 2 are ZHBs, respectively.

Binding energies between dimer constituents are greater for SB compared to NZ structures.

For [2Pro-H]⁻, [2Phe-H]⁻ and [2Glu-H]⁻, the binding energy difference between the SB and NZ

isomers is 49 kJ/mol, 34 kJ/mol and 64 kJ/mol, respectively. Thus, SB isomers are also stabilized

due to the energetic gain from dimer formation compared to NZ isomers.

However, the overall number of HBs and the binding energy in negative AA dimers can only

in part explain the energetic ordering of SB relative to NZ isomers. The Gibbs free energy

difference of SB minus NZ isomer at 0 K (ΔG_0) and 298 K (ΔG_{298}) is included in **Figure 3+4** to

the right of every NZ/SB isomer pair and summarized for different levels of theory in **Table S1**.

For the computational Gibbs free energy differences included in **Figure 3+4**, ΔG_{298} values as a

function of gas phase basicities summarized by Harrison[89] and Hunter/Lias[90] are shown in

Figure S5. There is a general trend in SB stability with increasing amino acid gas-phase basicity

for all amino acids except for His. His is 81 kJ/mol more basic than Cys yet the NZ isomer of

[2His-H]⁻ is more stable than the SB form by 20 kJ/mol. This unusual behavior for [2His-H]⁻ is

in line with the experimental IRMPD spectrum and indicates that maybe other structures than NZ

and SB shown in **Figure 4**, e.g., protonation of the His imidazole ring or imidazole⋯imidazole interactions, should be considered for [2His-H]⁻. However, none of these structures are computed to be energetically competitive with the low-energy SB/NZ isomers of [2His-H]⁻. The SB isomers of [2Cys-H]⁻ and [2Cys-3H]⁻ have more IHBs and ZHBs than the corresponding NZ isomers but the SB isomers are respectively 3 and 19 kJ/mol less stable than the NZ isomer. This is most likely due to the conformational constraints in [2Cys-3H]⁻ as a result of the disulfide bond preventing optimal SB formation, whereas one –SH group forms an additional HB to – COO⁻ in the SB isomer of [2Cys-H]⁻ (**Figure 3**). A similar effect occurs for [2Glu-H]⁻ for which the SB isomer is less stable than the NZ isomer by 1 kJ/mol (298 K) despite two additional ZHBs. SB isomers of [2Phe-H]⁻ and [2Pro-H]⁻, dimers of AAs with no HB donating or accepting groups in the side chain, are more stable than the corresponding NZ isomers by 18 kJ/mol and 5 kJ/mol (298 K), respectively. A similar conclusion for [2Phe-H]⁻ and [2Pro-H]⁻ is deduced from computational results using other levels of theory (**Table S1**).

These computational results suggest that the gas phase basicity, conformational constraints and hydrogen bond forming side chains all influence the relative stabilities of SB with respect to NZ isomers in negative AA dimers. SB isomers are thermodynamically more stable than the corresponding NZ isomers when the number of additional hydrogen bonds in SB compared to NZ isomers is high, and factors that interfere with SB bonding (such as interactions with side chain groups or conformational constraints) are absent, as in the case of [2Phe-H]⁻, [2Pro-H]⁻ and [2Gly-H]⁻.[66]

Comparisons to calculated spectra. The experimental spectra of [2Cys-H]⁻ and [2Cys-3H]⁻ (**Figure 5**), [2Glu-H]⁻ (**Figure 6**) and [2Pro-H]⁻ and [2Phe-H]⁻ (**Figure 7**) are shown along with computed linear IR spectra of low energy structures. Comparisons of the experimental spectra

with computed IR absorption spectra of alternative NZ or SB structures as well as with IR

spectra computed at different levels of theory are shown in **Figure S3-S4**, **S6-15**. Detailed

comparisons of the experimental band positions with predicted IR bands are summarized in

Table S2-S6. The IRMPD spectra of [2Cys-H]⁻ and [2Cys-3H]⁻ (**Figure 5a**, **5e**) are similar

indicating that –SH groups contribute only minimally to the experimental IRMPD spectrum of

[2Cys-H]⁻. Surprisingly, the predicted IR spectra of the NZ structures for [2Cys-H]⁻ and [2Cys-

3H]⁻ differ much more substantially. In the almost linearly extended structure of [2Cys-H]⁻, there

is no hydrogen bonding to the carboxylate's C=O group and the corresponding C=O stretch is

predicted at $\sim$1780 cm^{-1} whereas this band is observed experimentally at 1714 cm^{-1} (**Figure 5a**).

For the NZ structure of [2Cys-3H]⁻, the disulfide bridge enforces a conformation in which a

weak interaction between $-NH_2$ and C=O group shifts this band to $\sim$1730 cm^{-1} (**Figure 5f**) in

good agreement with the IRMPD spectrum (**Figure 5e**). For [2Cys-H]⁻, there are other higher

energy NZ isomers in which $-NH_2$ or –SH groups form hydrogen bonds to C=O and the band

position for these isomers is consistent with experimental results (**Figure S8-9**). For example, the

C=O band of the NZ* isomer shown in **Figure 5c**, which is 5 kJ/mol higher in energy than the

NZ structure and contains one additional HB between –SH and the carboxylate moiety compared

to the NZ isomer, is at 1708 cm^{-1}. This indicates that the band at 1690 – 1750 cm^{-1} in IRMPD

spectra (and its position in predicted IR spectra) of negative AA dimers is a very sensitive probe

for local changes in hydrogen bonding networks. For [2Cys-H]⁻ the assignment of the major

isomer that is present in the experimental ion population is ambiguous. Whereas the NZ structure

can be ruled out due to the poor agreement between experimental and calculated results, the

majority of experimental IRMPD bands are in line with the calculated spectra for the NZ* and

SB isomers. However, some bands are also missing in the experimental spectrum when

compared to the vibrational signatures for NZ* and SB isomers. For the SB isomer, the predicted strong $-NH_3^+$ umbrella (1480 cm^{-1}) and the corresponding stretching (1640 cm^{-1}) mode are absent in the IRMPD spectrum, whereas the $-O-H$ bending (1178 cm^{-1}) mode of the NZ* isomer is missing in the experimental spectrum. The low intensity of experimental bands compared to predicted $-O-H$ bending vibrations is consistent with previous IRMPD results for amino acid derivatives.[91,92] Most likely, the $-O-H$ bending vibration is significantly broadened in experiment because hydrogen bonding between $-OH$ and $-COO^-$ is predicted for NZ*. From results for proton bound AA dimers[42,46] broadening of $-NH_3^+$ modes that are involved in hydrogen bonding is also expected but especially the band at ~1480 cm^{-1} of the SB isomer could readily be resolved in experiment because no other experimental bands would interfere in this spectral region (**Figure 5a**). Therefore, both isomers, NZ* and SB, could co-exist in the experimental ion population but the absence of vibrations associated with $-NH_3^+$ hints to the NZ* isomer being the more abundant structure of [2Cys-H]$^-$. The comparison between theory and experiment for [2Cys-3H]$^-$ (**Figure 5e-g**) is more straightforward because the IR spectrum for the NZ (**Figure 5f**) isomer is clearly a better match for the experimental IRMPD spectrum than the SB (**Figure 5h**) and also NZ* (**Figure 5g**) structures and the result is in line with the predicted energetic ordering of the two isomers.

For [2Glu-H]$^-$, the experimental IRMPD spectrum is compared to predicted IR absorption spectra of NZ and SB structures in **Figure 6**. The SB structure is calculated to be lower in energy than the NZ structure at 0 K but destabilized at 298 K by 1 kJ/mol compared to the NZ isomer. For the ωB97-D/GCR level of theory, the SB structure is energetically favored over the NZ isomer at all temperatures (**Table S1**). Although there are minor differences between the calculated spectra for the NZ and SB structures, both structures are consistent with the

experimental spectrum. The only major difference between the calculated spectra is the high-frequency band. For the SB structure, the band is shifted to ~1700 cm^{-1}, whereas the band's maximum is located at ~1740 cm^{-1} for the NZ isomer consistent with the experimental spectrum. Due to the small energetic separation between NZ and SB structure for [2Glu-H]$^-$ and only minor differences between calculated spectra of these structures, the co-existence of both structures in the experimental ion population is possible but NZ structures are most likely more abundant than SB structures.

The experimental IRMPD spectra of [2Phe-H]$^-$ (**Figure 7a**) and [2Pro-H]$^-$ (**Figure 7e**) are compared with calculated spectra of NZ (Phe: **Figure 7b**; Pro: **Figure 7f**), higher energy NZ* (Phe: **Figure 7c**; Pro: **Figure 7g**) and SB (Phe: **Figure 7d**; Pro: **Figure 7h**) structures. For [2Phe-H]$^-$ and [2Pro-H]$^-$, the presence of the lowest energy NZ structure can be ruled out because the calculated spectra fail to explain almost all experimental IRMPD bands. For the high frequency band, this is again due to the absence of hydrogen bonding between –NH and C=O groups in these structures resulting in a blue shift of the C=O band in the calculated spectra. In contrast, the SB structure (**Figure 7d**) matches the experimental spectrum. Especially the feature at 1490 cm^{-1}, calculated to be the C-H in plane bend of the benzene ring coupled to the –NH$_3^+$ umbrella mode, and the experimental band at ~1580 cm^{-1} are in line with the SB structure. However, the presence of higher energy non-zwitterionic structure NZ* (**Figure 7c**) cannot be ruled out because it also matches the experimental IRMPD spectrum to some extent. For [2Pro-H]$^-$, the calculated spectrum of the SB structure (**Figure 7h**) is a much better match for the experimental result than the NZ* isomer (**Figure 7g**). In particular, the bands at 1691 cm^{-1}, 1604 cm^{-1} and 1360 cm^{-1} are in good agreement with calculated vibrational bands for the SB structure. This conclusion is also supported by calculated IR spectra using other levels of theory (**Figure**

S3). Therefore, these comparisons are in line with the presence of SB structures for [2Pro-H]⁻.

For both [2Phe-H]⁻ and [2Pro-H]⁻, some experimental bands are in line with computed IR bands of high-energy NZ* structures. Kinetic trapping of high-energy isomers as a result of solvent evaporation during ESI could explain the presence of NZ* structures in the experiments.[36] Kinetic trapping may favor formation of the NZ* but also SB isomers over NZ structures because NZ* complexes possess more HBs compared to NZ isomers and ZW AAs are more stable in solution and are potentially preserved in SB structures during ESI.

Conclusion

The binding between a neutral and a negatively charged AA in dimers, [2Xxx-H]⁻ (Xxx = Cys, Pro, Phe, His, Glu, Asp), [2Cys-3H]⁻, [Asp+Glu-H]⁻ and [2Glu-2H+Na]⁻, was investigated with IRMPD spectroscopy and theory. The spectra of the negative AA dimers are very similar and band positions and linewidths of spectral features differ only slightly between IRMPD spectra. The only exception is [2His-H]⁻ for which the IRMPD spectrum contains multiple bands that are not observed for the other complexes. This could indicate that the bonding arrangement between the AAs differs for [2His-H]⁻ from that of all other investigated negative AA dimers.

The IRMPD spectra for all other negatively charged AA dimers are qualitatively very similar suggesting that the bonding arrangements in these neutral-anion complexes to be also similar. All IRMPD bands are assigned based on previously reported condensed phase and gas phase IR spectra with the exception of [2Pro-H]⁻. For [2Pro-H]⁻, the high-frequency IRMPD band shifts to 1691 cm⁻¹. Only gas-phase spectra of proton bound AA dimers with strong $C=O^{\cdots+}H_3N-$ interactions or SB complexes can qualitatively explain this shift for Pro. Theoretical calculations for anionic AA dimers predict that either NZ or SB structures can be lowest in energy depending on the identity of the side chain, consistent with previous findings for [2Gly-H]⁻, which showed

that the SB form is most stable.[66] Extensive hydrogen bonding in AA dimer anions with no side chain functional groups and no steric or conformational interruption of AA binding are found to stabilize SB over NZ structures. These theoretical results are in line with the experimental IRMPD spectra. For [2Cys-H]⁻, [2Cys-3H]⁻ and [2Glu-H]⁻, comparisons between theory and experiment support preferential formation of NZ structures, whereas for [2Phe-H]⁻ and [2Pro-H]⁻, the presence of SB structures is invoked to explain the IRMPD spectra. Especially for [2Pro-H]⁻, only the lowest energy SB structure is able to explain the most intense bands and their positions in the experimental IRMPD spectrum.

These results clearly indicate that deprotonated AA dimers can form SB structures in the gas-phase if SB formation is not disrupted by side-chain interferences such as hydrogen bonding or conformational constrains. Although some of the investigated AAs are not involved in SBs in proteins, these results provide evidence for the role of hydrogen bonding in stabilizing SB interactions. This could potentially be important for peptide and protein environments where no interfering factors influence SB formation, such as protein-protein interfaces or the interior of proteins. Temperature dependent investigations of negative AA dimers with ion-mobility measurements to separate NZ and SB structures combined with IR spectroscopy should provide useful information about the propensity to form SB structures in these negatively charged ions in the gas phase as well as to investigate the influence of inter- and intramolecular interactions on SB stability in more detail.

Acknowledgements

Tables and Figures

Figure 1. IRMPD spectra of deprotonated AA dimers. Three reoccurring IR bands with high intensities are connected by dashed lines and the corresponding range of wavenumbers for which these bands are observed are included. Narrow features at ~1480 cm^{-1} for [2Phe-H]$^-$ and [2His-H]$^-$ are marked by black dots.
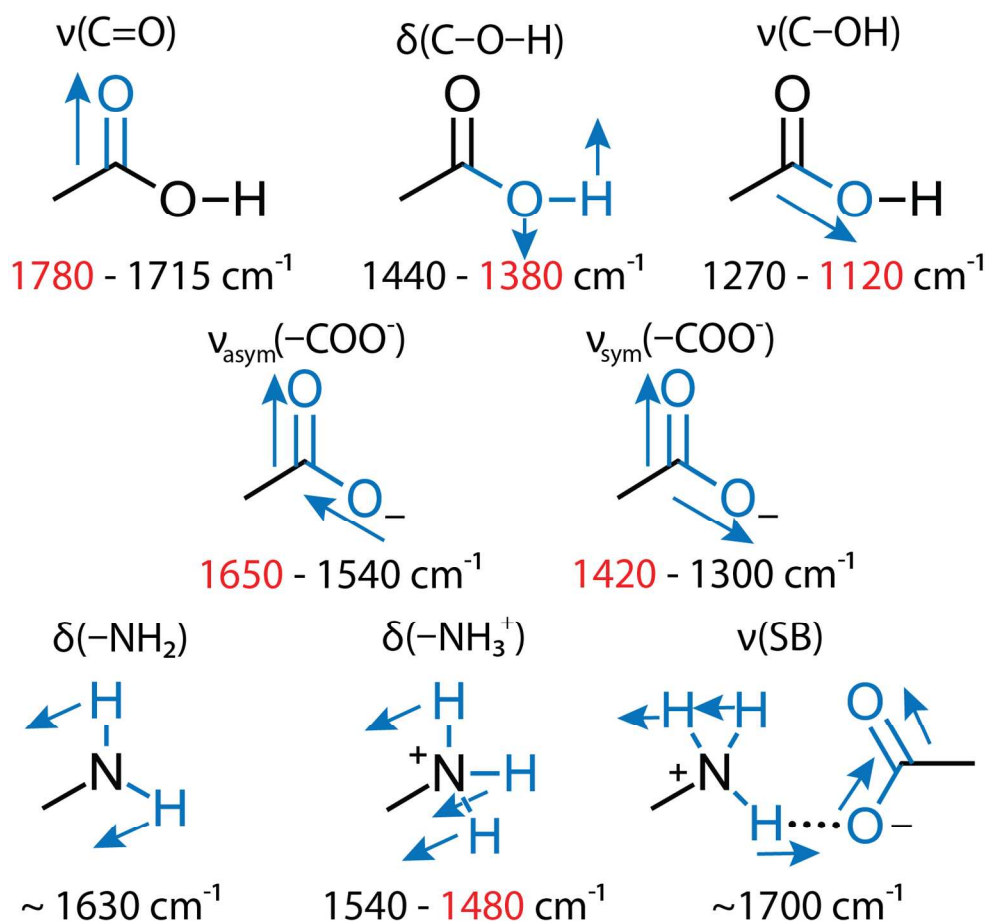
Figure 2. Sketch of the most important vibrational modes of negative amino acid dimers. For each mode the vibrationally active bonds/atoms and corresponding displacement vectors are shown in blue. The range of reported band positions are shown below each sketch (red: free vibration; black: maximum reported shift due to hydrogen bonding/non-covalent interactions).[7,8,46,72,75–80] For $\delta(-NH_2)$[75] and $\nu(SB)$ the scaled calculated band positions (B3LYP/GCR) are reported.
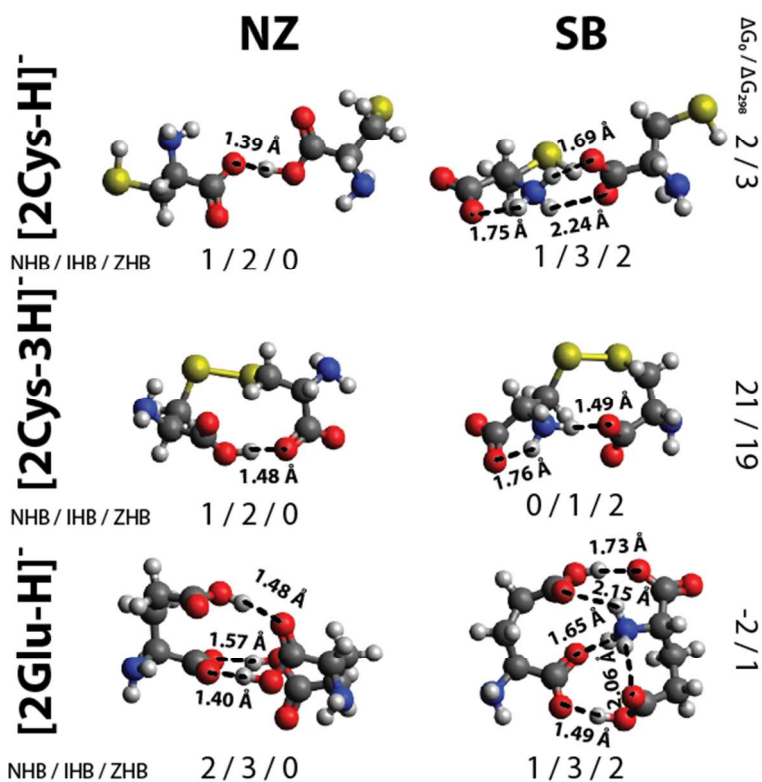
Figure 3. Lowest energy NZ and SB isomers of [2Cys-H]⁻, [2Cys-3H]⁻ and [2Glu-H]⁻. The shortest intermolecular and zwitterionic hydrogen bond lengths are included. The number of neutral hydrogen bonds (NHBs), ionic hydrogen bonds (IHBs) and zwitterionic hydrogen bonds (ZHBs) with bond length less than 2.30 Å are shown below every isomer. The Gibbs free energy differences in kJ/mol of the SB minus NZ isomer at 0 K (ΔG_0) and 298 K (ΔG_{298}) at the B3LYP/GCR level of theory are included. Oxygen, sulfur, nitrogen, carbon and hydrogen atoms are represented by red, yellow, blue, grey and white spheres, respectively.
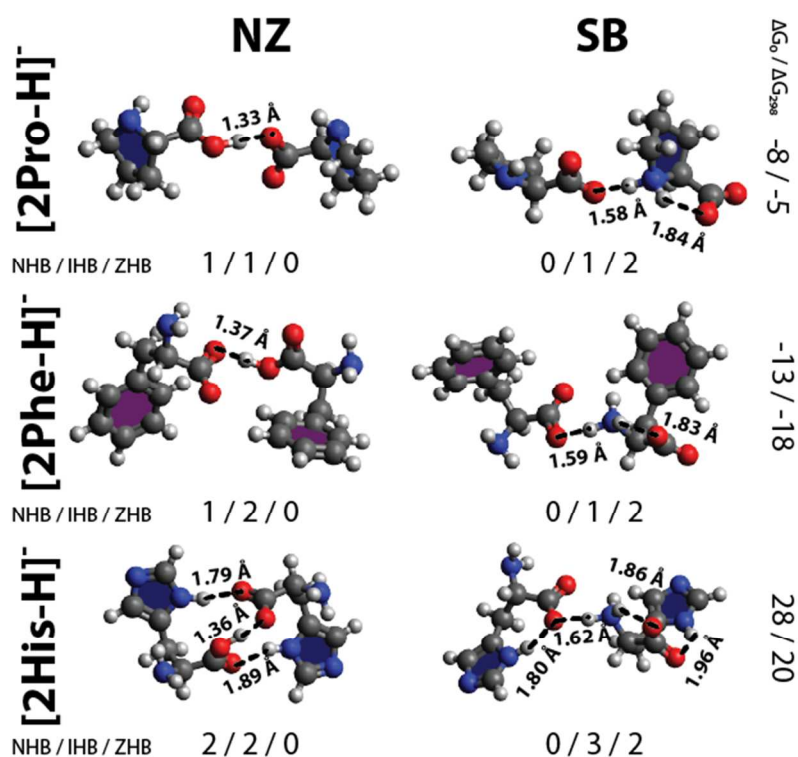
Figure 4. Lowest energy NZ and SB isomers of [2Pro-H]⁻, [2Phe-H]⁻ and [2His-H]⁻. The shortest intermolecular and zwitterionic hydrogen bond lengths are included. The number of neutral hydrogen bonds (NHBs), ionic hydrogen bonds (IHBs) and zwitterionic hydrogen bonds (ZHBs) with bond length less than 2.30 Å are shown below every isomer. The Gibbs free energy differences in kJ/mol of the SB minus NZ isomer at 0 K (ΔG_0) and 298 K (ΔG_{298}) at the B3LYP/GCR level of theory are included. Oxygen, sulfur, nitrogen, carbon and hydrogen atoms are represented by red, yellow, blue, grey and white spheres, respectively.
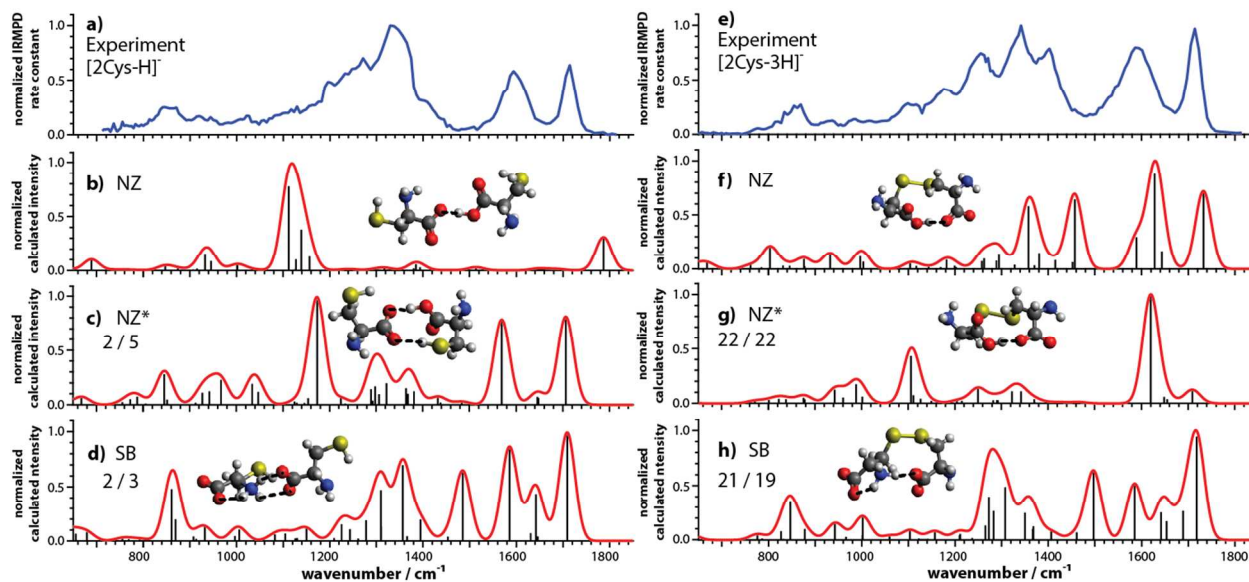
Figure 5. IRMPD spectra (a,e) and calculated IR spectra for low energy NZ (b,f), NZ* (c,g) and SB (d,h) structures of [2Cys-H]⁻ (b-d) and [2Cys-3H]⁻ (f-g). Gibbs free energy differences relative to the NZ structure at 0 K/298 K are included. Hydrogen bonds are indicated by dashed black lines.
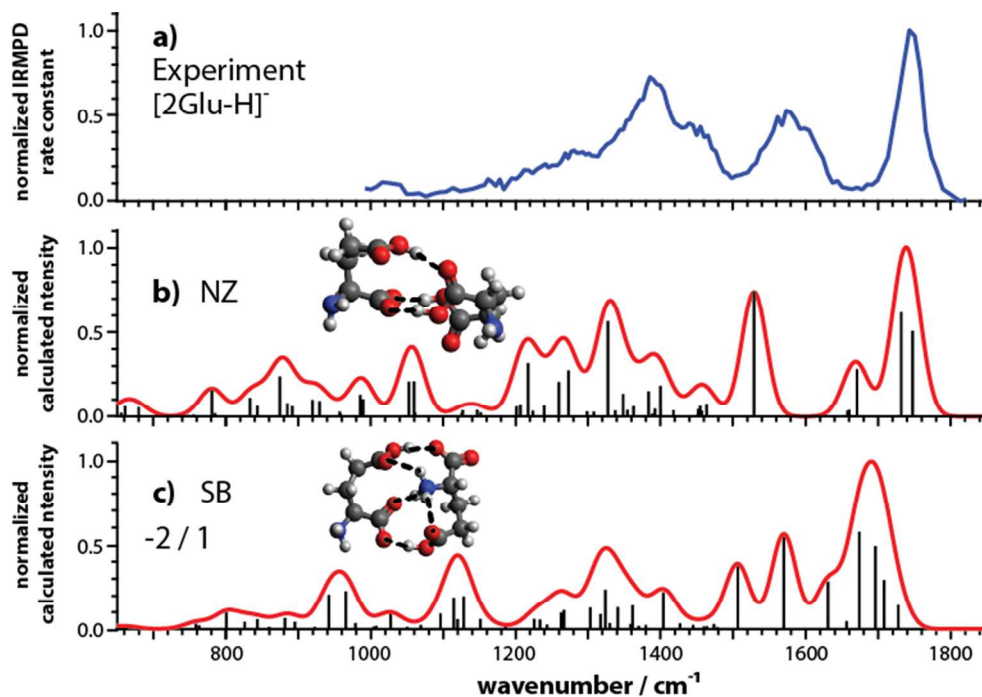
Figure 6. IRMPD spectrum (a) and calculated IR spectra for low energy NZ (b) and SB (c) structures of [2Glu-H]⁻ (a-c). Gibbs free energy differences at 0 K/298 K of the SB relative to the NZ isomer are included in c). Hydrogen bonds are indicated by dashed black lines.
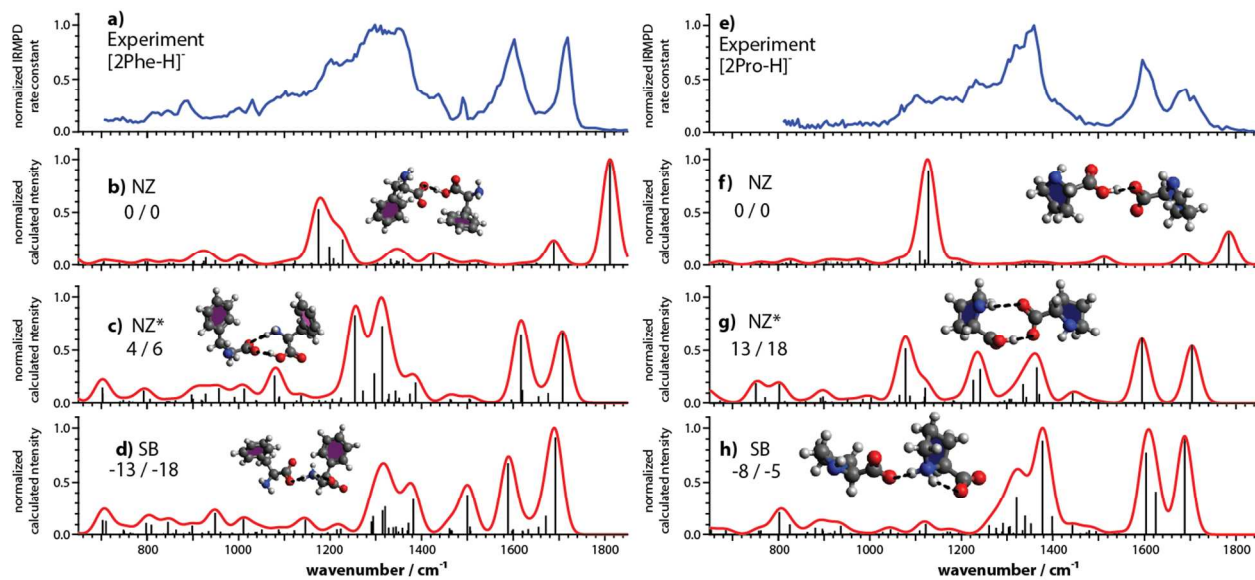
Figure 7. IRMPD spectra (a,e) and calculated IR spectra for low energy NZ (b,f), NZ* (c,g) and SB (d,h) structures of [2Phe-H]⁻ (b-d) and [2Pro-H]⁻ (f-g). Gibbs free energy differences relative to the NZ structure at 0 K/298 K are included. Hydrogen bonds are indicated by dashed black lines.

TOC Graphic
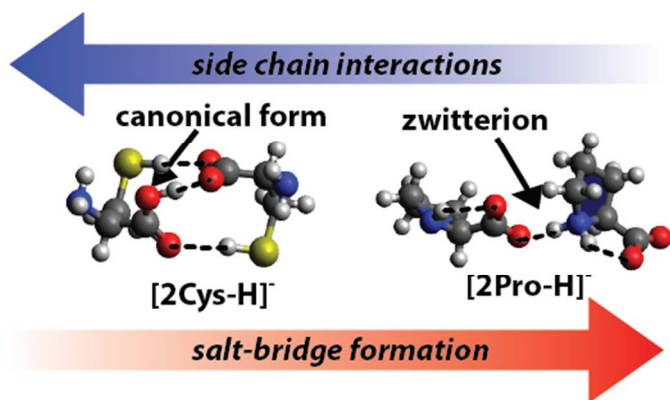
References

1   R. D. Suenram and F. J. Lovas, *J. Mol. Spectrosc.*, 1978, **72**, 372–382.

2   C. J. Chapo, J. B. Paul, R. A. Provencal, K. Roth and R. J. Saykally, *J. Am. Chem. Soc.*, 1998, **120**, 12956–12957.

3   Y. Ding and K. Krogh-Jespersen, *Chem. Phys. Lett.*, 1992, **199**, 261–266.

4   M. F. Bush, J. T. O'Brien, J. S. Prell, R. J. Saykally and E. R. Williams, *J. Am. Chem. Soc.*, 2007, **129**, 1612–1622.

5   M. W. Forbes, M. F. Bush, N. C. Polfer, J. Oomens, R. C. Dunbar, E. R. Williams and R. A. Jockusch, *J. Phys. Chem. A*, 2007, **111**, 11759–11770.

6   T. Wyttenbach, M. Witt and M. T. Bowers, *J. Am. Chem. Soc.*, 2000, **122**, 3458–3464.

7   P. B. Armentrout, M. T. Rodgers, J. Oomens and J. D. Steill, *J. Phys. Chem. A*, 2008, **112**, 2248–2257.

8   M. F. Bush, J. Oomens, R. J. Saykally and E. R. Williams, *J. Am. Chem. Soc.*, 2008, **130**, 6463–6471.

9   J. T. O'Brien, J. S. Prell, J. D. Steill, J. Oomens and E. R. Williams, *J. Phys. Chem. A*, 2008, **112**, 10823–10830.

10 M. T. Rodgers, P. B. Armentrout, J. Oomens and J. D. Steill, *J. Phys. Chem. A*, 2008, **112**, 2258–2267.

11 A. S. Lemoff, M. F. Bush and E. R. Williams, *J. Am. Chem. Soc.*, 2003, **125**, 13576–13584.

12 R. A. Coates, G. C. Boles, C. P. McNary, G. Berden, J. Oomens and P. B. Armentrout, *Phys. Chem. Chem. Phys.*, 2016, **18**, 22434–22445.

13 G. C. Boles, C. J. Owen, G. Berden, J. Oomens and P. B. Armentrout, *Phys. Chem. Chem. Phys.*, 2017, **19**, 12394–12406.

14 D. Corinti, B. Gregori, L. Guidoni, D. Scuderi, T. B. McMahon, B. Chiavarino, S. Fornarini and M. E. Crestoni, *Phys. Chem. Chem. Phys.*, 2018, **20**, 4429–4441.

15 J. T. O'Brien, J. S. Prell, G. Berden, J. Oomens and E. R. Williams, *Int. J. Mass Spectrom.*, 2010, **297**, 116–123.

16 M. Gutowski, P. Skurski and J. Simons, *J. Am. Chem. Soc.*, 2000, **122**, 10159–10162.

17 J. H. Jensen and M. S. Gordon, *J. Am. Chem. Soc.*, 1995, **117**, 8159–8170.

18 S. Xu, J. M. Nilles and K. H. Bowen, *J. Chem. Phys.*, 2003, **119**, 10696–10701.

19 M. F. Bush, J. S. Prell, R. J. Saykally and E. R. Williams, *J. Am. Chem. Soc.*, 2007, **129**, 13544–13553.

20 R. Wu and T. B. McMahon, *Angew. Chem. Int. Ed. Engl.*, 2007, **46**, 3668–3671.

21 R. Wu and T. B. McMahon, *J. Am. Chem. Soc.*, 2008, **130**, 3065–3078.

22 R. Wu and T. B. McMahon, *J. Mass Spectrom.*, 2008, **43**, 1641–1648.

23 A. C. Robinson, C. A. Castañeda, J. L. Schlessman and García-Moreno E. Bertrand, *Proc. Natl. Acad. Sci. U.S.A.*, 2014, **111**, 11685–11690.

24 F. O. Tzul, K. L. Schweiker and G. I. Makhatadze, *Proc. Natl. Acad. Sci. U.S.A.*, 2015, **112**, E259.

25 C. D. Waldburger, J. F. Schildbach and R. T. Sauer, *Nat. Struct. Biol.*, 1995, **2**, 122 EP -.

26 M. Shimaoka, T. Xiao, J.-H. Liu, Y. Yang, Y. Dong, C.-D. Jun, A. McCormack, R. Zhang, A. Joachimiak, J. Takagi, J.-H. Wang and T. A. Springer, *Cell*, **112**, 99–111.

27 A. Purohit, J. K. England, L. G. Douma, F. Tondnevis, L. B. Bloom and M. Levitus, *Biophys. J.*, 2017, **113**, 794–804.

28 Z. Zhang, S. J. Browne and R. W. Vachet, *J. Am. Soc. Mass Spectrom.*, 2014, **25**, 604–613.

29 Z. Zhang and R. W. Vachet, *Int. J. Mass Spectrom.*, 2017, **420**, 51–56.

30 Loo, Rachel R. Ogorzalek and J. A. Loo, *J. Am. Soc. Mass Spectrom.*, 2016, **27**, 975–990.

31 G. C. Donohoe, M. Khakinejad and S. J. Valentine, *J. Am. Soc. Mass Spectrom.*, 2015, **26**, 564–576.

32 J. Bonner, Y. A. Lyon, C. Nellessen and R. R. Julian, *J. Am. Chem. Soc.*, 2017, **139**, 10286–10293.

33 P. D. Schnier, W. D. Price, R. A. Jockusch and E. R. Williams, *J. Am. Chem. Soc.*, 1996, **118**, 7178–7189.

34 D. Mao and Douglas, D. J., *J. Am. Soc. Mass Spectrom.*, 2003, **14**, 85–94.

35 T. Wyttenbach, G. von Helden and M. T. Bowers, *J. Am. Chem. Soc.*, 1996, **118**, 8355–8364.

36 G. Papadopoulos, A. Svendsen, O. V. Boyarkin and T. R. Rizzo, *J. Am. Soc. Mass Spectrom.*, 2012, **23**, 1173–1181.

37 C. F. Rodriquez, G. Orlova, Y. Guo, X. Li, C.-K. Siu, A. C. Hopkinson and Siu, K. W. Michael, *J. Phys. Chem. B*, 2006, **110**, 7528–7537.

38 E. F. Strittmatter and E. R. Williams, *J. Phys. Chem. A*, 2000, **104**, 6069–6076.

39 R. R. Julian and M. F. Jarrold, *J. Phys. Chem. A*, 2004, **108**, 10861–10864.

40 S.-W. Lee, H. S. Kim and Beauchamp, J. L., *J. Am. Chem. Soc.*, 1998, **120**, 3188–3195.

41 N. C. Polfer, B. Paizs, L. C. Snoek, I. Compagnon, S. Suhai, G. Meijer, G. von Helden and J. Oomens, *J. Am. Chem. Soc.*, 2005, **127**, 8571–8579.

42 C. Ieritano, P. J. J. Carr, M. Hasan, M. Burt, R. A. Marta, V. Steinmetz, E. Fillion, T. B. McMahon and W. Scott Hopkins, *Phys. Chem. Chem. Phys.*, 2016, **18**, 4704–4710.

43 W. D. Price, P. D. Schnier and E. R. Williams, *J. Phys. Chem. B*, 1997, **101**, 664–673.

44 C. G. Atkins, K. Rajabi, E. A. L. Gillis and T. D. Fridgen, *J. Phys. Chem. A*, 2008, **112**, 10220–10225.

45 X. Kong, I.-A. Tsai, S. Sabu, C.-C. Han, Y. T. Lee, H.-C. Chang, S.-Y. Tu, A. H. Kung and C.-C. Wu, *Angew. Chem. Int. Ed. Engl.*, 2006, **45**, 4130–4134.

46 J. Seo, W. Hoffmann, S. Malerz, S. Warnke, M. T. Bowers, K. Pagel and G. von Helden, *Int. J. Mass Spectrom.*, 2017, https://doi.org/10.1016/j.ijms.2017.06.011.

47 R. Wu and T. B. McMahon, *J. Am. Chem. Soc.*, 2007, **129**, 4864–4865.

48 W. D. Price, R. A. Jockusch and E. R. Williams, *J. Am. Chem. Soc.*, 1997, **119**, 11988–11989.

49 J. T. O'Brien, J. S. Prell, J. D. Steill, J. Oomens and E. R. Williams, *J. Am. Chem. Soc.*, 2009, **131**, 3905–3912.

50 Y. J. Alahmadi, A. Gholami and T. D. Fridgen, *Phys. Chem. Chem. Phys.*, 2014, **16**, 26855–26863.

51 R. A. Jockusch, W. D. Price and E. R. Williams, *J. Phys. Chem. A*, 1999, **103**, 9266–9274.

52 R. R. Julian, Beauchamp, J. L. and W. A. Goddard, *J. Phys. Chem. A*, 2002, **106**, 32–34.

53 J. S. Prell, J. T. O'Brien, J. D. Steill, J. Oomens and E. R. Williams, *J. Am. Chem. Soc.*, 2009, **131**, 11442–11449.

54 J. S. Prell, M. Demireva, J. Oomens and E. R. Williams, *J. Am. Chem. Soc.*, 2009, **131**, 1232–1242.

55 J. M. Talley, B. A. Cerda, G. Ohanessian and C. Wesdemiotis, *Chem. Eur. J.*, 2002, **8**, 1377–1388.

56 C. Kapota, J. Lemaire, P. Maître and G. Ohanessian, *J. Am. Chem. Soc.*, 2004, **126**, 1836–1842.

57 U. J. Lorenz and T. R. Rizzo, *J. Am. Chem. Soc.*, 2012, **134**, 11053–11055.

58 H.-B. Oh, C. Lin, H. Y. Hwang, H. Zhai, K. Breuker, V. Zabrouskov, B. K. Carpenter and F. W. McLafferty, *J. Am. Chem. Soc.*, 2005, **127**, 4076–4083.

59 K. Rajabi and T. D. Fridgen, *J. Phys. Chem. A*, 2008, **112**, 23–30.

60 H. Yin and X. Kong, *J. Am. Soc. Mass Spectrom.*, 2015, **26**, 1455–1461.

61 R. Wu, R. A. Marta, J. K. Martens, K. R. Eldridge and T. B. McMahon, *J. Am. Soc. Mass Spectrom.*, 2011, **22**, 1651.

62 M. Citir, C. S. Hinton, J. Oomens, J. D. Steill and P. B. Armentrout, *J. Phys. Chem. A*, 2012, **116**, 1532–1541.

63 I. Gitlin, J. D. Carbeck and G. M. Whitesides, *Angew. Chem. Int. Ed.*, 2006, **45**, 3022–3060.

64 E. M. Milner, Nix, Michael G. D. and Dessent, Caroline E. H., *J. Phys. Chem. A*, 2012, **116**, 801–809.

65 T. M. Chang, G. Berden, J. Oomens and E. R. Williams, *Int. J. Mass Spectrom.*, 2015, **377**, 440–447.

66 S. Heiles, R. J. Cooper, G. Berden, J. Oomens and E. R. Williams, *Phys. Chem. Chem. Phys.*, 2015, **17**, 30642–30647.

67 A. M. Rijs, G. Ohanessian, J. Oomens, G. Meijer, G. von Helden and I. Compagnon, *Angew. Chem. Int. Ed. Engl.*, 2010, **49**, 2332–2335.

68 N. L. Burke, A. F. DeBlase, J. G. Redwine, J. R. Hopkins, S. A. McLuckey and T. S. Zwier, *J. Am. Chem. Soc.*, 2016, **138**, 2849–2857.

69 Y. Shao, Z. Gan, E. Epifanovsky, A. T. Gilbert, M. Wormit, J. Kussmann, A. W. Lange, A. Behn, J. Deng, X. Feng, D. Ghosh, M. Goldey, P. R. Horn, L. D. Jacobson, I. Kaliman, R. Z. Khaliullin, T. Kuś, A. Landau, J. Liu, E. I. Proynov, Y. M. Rhee, R. M. Richard, M. A. Rohrdanz, R. P. Steele, E. J. Sundstrom, H. L. Woodcock, P. M. Zimmerman, D. Zuev, B. Albrecht, E. Alguire, B. Austin, G. J. O. Beran, Y. A. Bernard, E. Berquist, K. Brandhorst, K. B. Bravaya, S. T. Brown, D. Casanova, C.-M. Chang, Y. Chen, S. H. Chien, K. D. Closser, D. L. Crittenden, M. Diedenhofen, R. A. DiStasio, H. Do, A. D. Dutoi, R. G. Edgar, S. Fatehi, L. Fusti-Molnar, A. Ghysels, A. Golubeva-Zadorozhnaya, J. Gomes, M. W. Hanson-Heine, P. H. Harbach, A. W. Hauser, E. G. Hohenstein, Z. C. Holden, T.-C. Jagau, H. Ji, B. Kaduk, K. Khistyaev, J. Kim, J. Kim, R. A. King, P. Klunzinger, D. Kosenkov, T. Kowalczyk, C. M. Krauter, K. U. Lao, A. D. Laurent, K. V. Lawler, S. V. Levchenko, C. Y. Lin, F. Liu, E. Livshits, R. C. Lochan, A. Luenser, P. Manohar, S. F. Manzer, S.-P. Mao, N. Mardirossian, A. V. Marenich, S. A. Maurer, N. J. Mayhall, E. Neuscamman, C. M. Oana, R. Olivares-Amaya, D. P. O'Neill, J. A. Parkhill, T. M. Perrine, R. Peverati, A. Prociuk, D. R. Rehn, E. Rosta, N. J. Russ, S. M. Sharada, S. Sharma, D. W. Small, A. Sodt, T. Stein, D. Stück, Y.-C. Su, A. J. Thom, T. Tsuchimochi, V. Vanovschi, L. Vogt, O. Vydrov, T. Wang, M. A. Watson, J. Wenzel, A. White, C. F. Williams, J. Yang, S. Yeganeh, S. R. Yost, Z.-Q. You, I. Y. Zhang, X. Zhang, Y. Zhao, B. R. Brooks, G. K. Chan, D. M. Chipman, C. J. Cramer, W. A. Goddard, M. S. Gordon, W. J. Hehre, A. Klamt, H. F. Schaefer, M. W. Schmidt, C. D. Sherrill, D. G. Truhlar, A. Warshel, X. Xu, A. Aspuru-Guzik, R. Baer, A. T. Bell, N. A. Besley, J.-D. Chai, A. Dreuw, B. D. Dunietz, T. R. Furlani, S. R. Gwaltney, C.-P. Hsu, Y. Jung, J. Kong, D. S. Lambrecht, W. Liang, C. Ochsenfeld, V. A. Rassolov, L. V. Slipchenko, J. E. Subotnik, T. van Voorhis, J. M. Herbert, A. I. Krylov, P. M. Gill and M. Head-Gordon, *Mol. Phys.*, 2014, **113**, 184–215.

70 J.-D. Chai and M. Head-Gordon, *Phys. Chem. Chem. Phys.*, 2008, **10**, 6615–6620.

71 F. B. van Duijneveldt, J. G. C. M. van Duijneveldt-van de Rijdt and J. H. van Lenthe, *Chem. Rev.*, 1994, **94**, 1873–1885.

72 J. Seo, J. Jang, S. Warnke, S. Gewinner, W. Schöllkopf and G. von Helden, *J. Am. Chem. Soc.*, 2016, **138**, 16315–16321.

73 C. M. Leavitt, A. B. Wolk, M. Z. Kamrath, E. Garand, M. J. van Stipdonk and M. A. Johnson, *J. Am. Soc. Mass Spectrom.*, 2011, **22**, 1941–1952.

74 K. R. Asmis, N. L. Pivonka, G. Santambrogio, M. Brümmer, C. Kaposta, D. M. Neumark and L. Wöste, *Science*, 2003, **299**, 1375.

75 J. Oomens, J. D. Steill and B. Redlich, *J. Am. Chem. Soc.*, 2009, **131**, 4310–4319.

76 E. Spinner, *J. Chem. Soc.*, 1964, 4217.

77 E. Spinner, *J. Chem. Soc., B:*, 1967, 874.

78 J. Oomens and J. D. Steill, *J. Phys. Chem. A*, 2008, **112**, 3281–3283.

79 M. M. Quesada-Moreno, J. R. Avilés-Moreno, A. Á. Márquez-García, F. Partal-Ureña and J. J. López González, *J. Mol. Struct.*, 2013, **1046**, 136–146.

80 M. F. Bush, M. W. Forbes, R. A. Jockusch, J. Oomens, N. C. Polfer, R. J. Saykally and E. R. Williams, *J. Phys. Chem. A*, 2007, **111**, 7753–7760.

81 N. C. Polfer, J. Oomens, D. T. Moore, G. von Helden, G. Meijer and R. C. Dunbar, *J. Am. Chem. Soc.*, 2006, **128**, 517–525.

82 M. K. Drayß, P. B. Armentrout, J. Oomens and M. Schäfer, *Int. J. Mass Spectrom.*, 2010, **297**, 18–27.

83 F. Lanucara, B. Chiavarino, M. E. Crestoni, D. Scuderi, R. K. Sinha, P. Maître and S. Fornarini, *Int. J. Mass Spectrom.*, 2012, **330-332**, 160–167.

84 R. C. Dunbar, J. Oomens, G. Berden, J. K.-C. Lau, U. H. Verkerk, A. C. Hopkinson and Siu, K. W. Michael, *J. Phys. Chem. A*, 2013, **117**, 5335–5343.

85 Marcia Cordes, de N. D. and J. L. Walter, *Spectrochim. Actra, Part A*, 1968, **24**, 237–252.

86 M. Meot-Ner, *Chem. Rev.*, 2005, **105**, 213–284.

87 M. Meot-Ner Mautner, *Chem. Rev.*, 2012, **112**, PR22-103.

88 C. L. Perrin and J. B. Nielson, *Annu. Rev. Phys. Chem.*, 1997, **48**, 511–544.

89 A. G. Harrison, *Mass Spectrom. Rev.*, 1997, **16**, 201–217.

90 E. P. L. Hunter and S. G. Lias, *J. Phys. Chem. Ref. Data*, 1998, **27**, 413–656.

91 D. Corinti, A. De Petris, C. Coletti, N. Re, B. Chiavarino, M. E. Crestoni and S. Fornarini, *ChemPhysChem*, 2017, **18**, 318–325.

92 R. Paciotti, C. Coletti, N. Re, D. Scuderi, B. Chiavarino, S. Fornarini and M. E. Crestoni, *Phys. Chem. Chem. Phys.*, 2015, **17**, 25891–25904.